An investigation of dynamic crack initiation in PMMA

Daniel Rittel, Hubert Maigre

An investigation of dynamic crack initiation in PMMA

D. Rittel [a,*], H. Maigre [b]

[a] *Faculty of Mechanical Engineering, Technion, 32000 Haifa, Israel*
[b] *Laboratoire de Mécanique des Solides, U A 317 CNRS Ecole Polytechnique, F-91128 Palaiseau Cedex, France*

The recently developed compact compression specimen (CCS) — H integral technique is applied to the characterization of the dynamic fracture toughness of PMMA under transient loading. The forces and displacements on the boundaries of a cracked CCS are applied and determined using a Kolsky apparatus. The path-independent H-integral is thus calculated by forming a convolution product between experimental and reference data. The evolution of both the mode I and mode II stress intensity factors is determined by solving linear convolution equations. Therefore, the history of the stress intensity factors is assessed from the onset of loading until early crack propagation detected by a fracture gage. Dynamic fracture toughness is taken as the value of the mode I stress intensity factor at fracture time. Experimental results compare well with previously reported values while extending the range of applied loading rates. The fracture toughness is observed to increase markedly with the stress intensity rate. This observation is discussed in the light of fractographic examination showing the existence of a characteristic rough zone directly ahead of the notch-tip of dynamically fractured specimens.

Keywords: Dynamic fracture toughness; Stress intensity factor; Compact compression specimen; H-integral; Mixed mode fracture; PMMA; Kolsky bar

1. Introduction

Estimation of dynamic mechanical properties of materials is important to the designer since these properties, such as the yield strength, can be quite different from their static counterparts. Regarding fracture properties, whereas the static fracture toughness K_{Ic} is now assessed using standard procedures (e.g. ASTM, 1993), the dynamic fracture toughness K_{Id}^{c} is still evaluated in a variety of experimental procedures (for a review, see Kobayashi, 1987; Kalthoff, 1990).

Bui and Maigre (1988) introduced the path-independent dynamic H-integral which relates the stress intensity factors to the externally applied loads and displacements. This concept was further developed and implemented experimentally using the compact compression specimen (CCS) (Bui et al., 1992; Rittel et al., 1992). The evolution of the mode I stress intensity factor was determined on a steel specimen from the onset of loading until early crack propagation detected by a single-wire fracture gage (Rittel et al., 1992). The procedure was extended to apply to the simultaneous characterization of mode I and mode II SIF's (Maigre and Rittel, 1993). In addition to the information provided by the fracture gages, the onset of crack propagation was characterized by

* Corresponding author. Tel.: +972-4-8293261; fax: +972-4-8324533; e-mail: merittel@techunix.technion.ac.il.

taking advantage of the reciprocity between the measured forces and displacements on the boundary of the specimen. Reciprocity implies that the evolutions of the stress intensity factors formulated in terms of either forces or displacements should be identical until fracture occurs (Maigre and Rittel, 1995).

Therefore, the framework consisting of the H-integral and the compact compression specimen is quite convenient for the testing of a relatively large sample size with minimum experimental and numerical investment (Rittel and Maigre, 1993).

Brittle polymers have often been studied as model materials in dynamic fracture studies. However the sample size is generally relatively small while different researchers use different frameworks (theoretical and experimental). It has been observed that the dynamic fracture toughness increases with the stress intensity rate (Ravi-Chandar and Knauss, 1984; Wada, 1992) but the mechanisms underlying this dependence are not clear. Furthermore few attempts have been made to correlate and compare the results obtained by different researchers using different techniques.

Consequently, this paper reports and extends results on dynamic crack initiation in commercial PMMA using the compact compression specimen technique. The present results are compared with previously reported results on a similar material. Fractographic characterization of the specimens is carried out and features which are characteristic of dynamic crack initiation are reported and related to the measured fracture parameters.

The paper is organized as follows: first, we briefly recall the basic principles of the approach and its experimental application. Next specific experimental aspects of this study are addressed. Then we present the results obtained on 17 PMMA specimens, namely the dynamic fracture toughness and the results of the fractographic characterization of the specimens. These results are discussed in the light of previously reported results.

2. The H-integral and the compact compression specimen

The H-integral is a path-independent integral which relates forces ($\underline{T}$) and displacements ($\underline{u}$ and $\underline{v}$) on the external boundaries S of a cracked solid (crack length a) to the stress intensity factors K_{I} and K_{II} (Bui and Maigre, 1988). This concept applies to 2D linear-elastic media. In this integral the time dependence is explicitly taken into account through

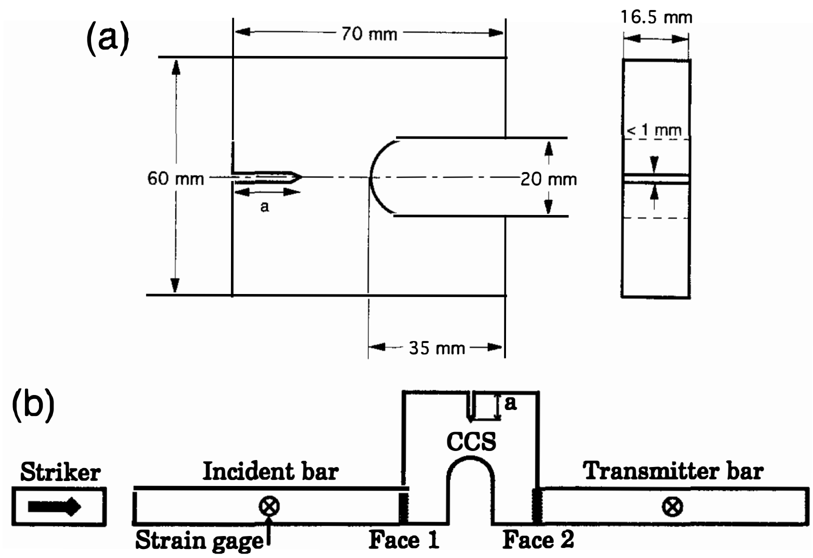

Fig. 1. (a) The compact Compression Specimen (CCS). (b) Experimental setup: the CCS is inserted between two instrumented bars (Kolsky bar). Transient signals are recorded on the two strain gages to determine interfacial (face 1 and face 2) forces and displacements.

convolution products (noted $*$). The general expression for H is as follows:

$$H(\tau) := \frac{1}{2}\int_S \left\{ \underline{T}[\underline{u}] * \frac{\partial \underline{v}}{\partial a} - \frac{\partial \underline{T}[\underline{v}]}{\partial a} * \underline{u} \right\} \mathrm{d}S$$

$$= \frac{1-\nu^2}{E} K^{u}_{\alpha \mathrm{d}} * K^{v}_{\alpha \mathrm{d}} \quad \alpha = \mathrm{I}, \mathrm{II} \tag{1}$$

A simpler expression is obtained by assuming constant applied forces with respect to the crack length variation. Let the subscript *ref* denote reference data (calculated numerically), while *exp* indicates experimental data. With E and ν denoting Young's modulus and Poisson's ratio respectively, H can be written as follows:

$$H(\tau) = \frac{1}{2}\int_S \underline{T}^{\exp} * \frac{\partial \underline{u}^{\mathrm{ref}}}{\partial a} \mathrm{d}S = \frac{1-\nu^2}{E} K^{\exp}_{\alpha \mathrm{d}} * K^{\mathrm{ref}}_{\alpha \mathrm{d}}$$

$$\alpha = \mathrm{I}, \mathrm{II} \tag{2}$$

Practically, the determination of $K_{\alpha \mathrm{d}}$ amounts to solving a linear convolution equation, once H has been estimated (from the forces and displacements) and the corresponding references calculated. The contribution of each crack opening mode can now be ascertained the following way: H is separated into its pure mode I and mode II components using reference data corresponding to each mode. Finally, the required SIF is determined by solving the corresponding (I or II) linear convolution equation.

Experimentally, we use a split Hopkinson bar (Kolsky bar) to apply dynamic loads and measure interfacial displacements (Follansbee, 1985). A convenient specimen geometry is provided by the CCS which can be inserted between the bars and loaded without extra devices to turn compression into tension (Fig. 1, Rittel and Maigre, 1993). The onset of crack propagation is detected by single wire fracture gages. It can be noted that the geometry of the CCS is symmetric, but loads are applied on one side only. Consequently, one can assume that mode I is the predominant crack opening mode keeping in mind that a certain amount of mode II is present. For a given series of experiments, one has to generate a couple of reference data (mode I and mode II) for *any* crack length between a and $a + \mathrm{d}a$. This way, the contribution of each mode can be assessed quantitatively until fracture time (Maigre and Rittel, 1993). The method is simple to implement experimentally. Furthermore, since the set of references must be generated only once for a series of experiments, a large sample size can be tested.

Table 1
Measured mechanical properties of the commercial PMMA used in this study

	Young's modulus (GPa)	Poisson's ratio
Static	3.70	0.42
Dynamic	5.76	0.42

3. Material and experimental

This study was carried out on commercial PMMA ($\rho = 1182$ kg/m^3) whose properties (as measured in our laboratory) are listed in Table 1. Since PMMA is a viscous material, a transfer modulus was determined by measuring the time required for waves to travel in a rod specimen (Zhao, 1992). Such transfer modulus (although of lower value) was also employed by other researchers in a similar case (Wada, 1992; Wada et al., 1992). Compact compression specimens were all manufactured from the same plate and care was exerted to have all slits oriented in the same direction. Sharp notches (average root radius 0.2 mm) were machined mechanically and no attempt was made to obtain sharper notches. The degree of material isotropy was assessed by measuring ultrasonic wave velocity (at 1 and 0.5 MHz) parallel and through the thickness with respect to the notch. These measurements showed very little difference between the two directions so that the material can reasonably be considered as isotropic, at least for computational purposes.

Two specimens were used to determine the static fracture toughness of the material. The specimens were slowly loaded in compression. A 2D finite element model was used to calculate the SIF at fracture (K_{Ic}) using Irwin's formula which relates the crack opening displacement (COD) to the SIF

$$COD(r, \Theta = \Pi) = K_{\mathrm{I}} \frac{8(1-\nu)^2}{E} \sqrt{\frac{r}{2\Pi}}. \tag{3}$$

Dynamic testing was carried out on 16.5 mm diameter maraging steel bars. A total of 15 specimens were tested. A single wire commercial fracture gage (MM CD 02 15A) was glued in the vicinity of the notch tip. In some cases, we used one gage on each face of the specimen. As the crack propagated, it fractured the wire and triggered a pulse on the recording system. All signals were synchronized with the signals of the incident gage and sampling was carried out at 1 MHz. The difference in position of the fracture gage with respect to the crack-tip was assessed 'post mortem'. It was noted that this difference rarely exceeded 0.2 mm. Gage signals were corrected for geometric dispersion and processed to determine interfacial forces and displacements using DAVID program (Gary and Klepaczko, 1988). The duration of the impact, as set by the length of the impacter, was 70 or 350 μs. In a couple of cases, we used a small steel ball to achieve a shorter impact (about 30 μs). However in that case the impact pulse was gaussian rather than square shaped.

For three specimens (P6, P8 and P9), the (average) initial crack velocity was monitored using a commercial fracture gage. This provided additional data to the fracture toughness.

Finally, in one case (specimen P17), we carried out an experiment without the transmitter bar. The experiment was successful, in that the specimen fractured as it happens in one point bend experiments (Giovanola, 1986). For all specimens except P17, fracture was observed to proceed along the initial notch line whereas for specimen P17 the crack propagated by forming at a kink angle of about 45°.

For each experiment, the amount of mode II contribution was assessed. Also, the rate of loading was specified as the value of the mode I fracture toughness divided by the time to fracture. Time to fracture is defined as the 'active' loading time during which the crack opens effectively until fracture.

4. Results

4.1. Dynamic fracture toughness

Typical experimental signals (incident pulse, interfacial forces and time to fracture) are shown in Fig. 2 (Maigre and Rittel, 1995). Here, the incident

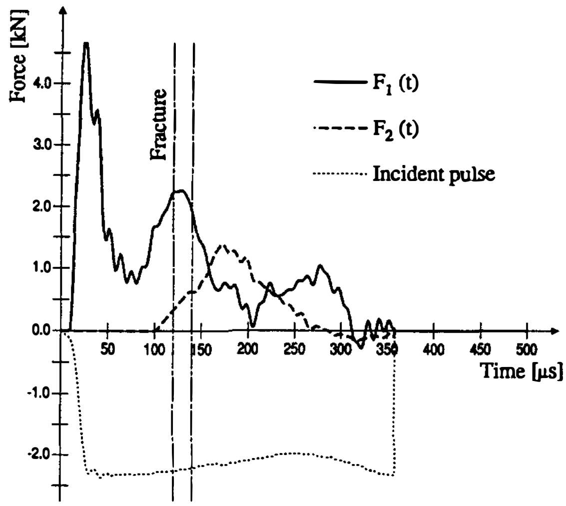

Fig. 2. Typical experimental signals (specimen P16). Incident pulse (arbitrary units) and interfacial forces. Fracture is detected by 2 gages. Note that fracture occurred before completion of the incident pulse.

pulse lasts about 350 μs. The signal takes typically 60–70 μs to reach the crack and force its opening. Fracture occurs soon after. A common feature to all tests is that fracture occurs well before completion of the 350 μs. Consequently, the specimen cannot withstand the entire signal, as it appears on the interfacial incident force pulse. It can thus be concluded that the first passage of the wave causes fracture before the pulse could leave the specimen through the transmitter bar interface. Fracture occurs in a truly dynamic mode, in other words the transmitter bar is not really needed in this series of experiments. This observation was confirmed by the successful testing of specimen P17 which fractured due to inertia only. Fig. 3 shows the a typical evolution of $K_{Id}(t)$ and $K_{IId}(t)$ until fracture. These results are obtained by the linear deconvolution procedure. This evolution can be considered as typical in the sense that mode I was observed to be systematically dominant in all the experiments reported here. However, the picture might be different for materials (specimens) which fracture in very short times as noted by Kalthoff and Podleschny (1992).

In Table 2 we have listed the experimental values of the fracture toughness, $K_{Id}^{c} = K_{Id}(t)$ at $t = t_{frac}$ along with the stress intensity rate $\dot{K}_{Id}$ These results are plotted in Fig. 4(a). Although various configura-

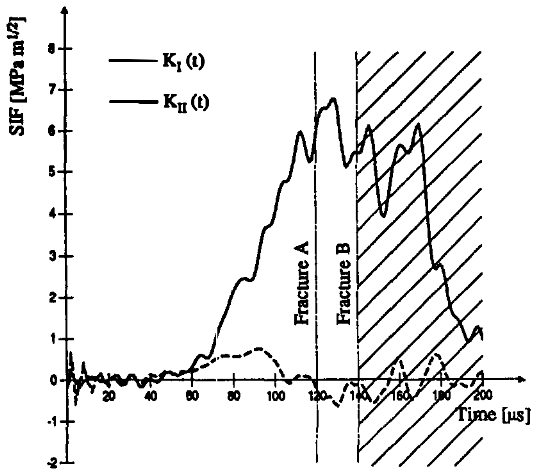

Fig. 3. Specimen P16. Evolution of mode I and mode II dynamic stress intensity factors. Note that mode I is predominant during most of the test. Results are not valid past fracture time.

tions of crack length and pulse duration were tested, it seems that these factors did not affect the results. On the contrary a common trend for all specimens can be observed: the dynamic fracture toughness increases markedly with the stress intensity rate. Moreover, the dynamic values are larger than the static ones.

In Fig. 4(b) we have plotted our results together with those obtained by Wada (1992) and Wada et al. (1992) (Rittel and Maigre, 1993). These researchers worked on a slightly different material (lower static fracture toughness) with perhaps sharper cracks. They also used a hybrid experimental–numerical approach and one point bend specimens ensuring almost perfect mode I loading. Yet, in spite of the different experimental methods, it can be noted that our results compare very well with theirs in the common range of stress intensity rates, i.e. 5.0×10^4–1.0×10^5 MPa $\sqrt{m}$/s. It should also be noted that in the present work, we could reach higher stress intensity rates thus extending the range of experimental data.

Finally, we have listed in Table 3 three values of fracture toughness and the corresponding measured average velocity. A good correlation between these two sets of data can be noticed, in the sense that the initial crack velocity increases with the dynamic fracture toughness. This result can be qualitatively understood in terms of energy stored ahead of the crack-tip prior to its extension but this point is beyond the scope of our study.

4.2. Fractographic examination

4.2.1. Macroscopic

The last column of Table 2 refers to the macroscopic aspect of the fracture surface of the specimens

Table 2
Experimental results. $\bar{a}$ indicates average crack length. In the rightmost column, M refers to 'mirror/mist' and H to 'hackles' in the vicinity of the crack-tip. When two gages were used, two values are reported consistently for each fracture parameter

Specimen	$\bar{a}$ [mm]	t_{frac} [μs]	K_{Id}^c (MPa $\sqrt{m}$)	$\dot{K}_{Id}$ (MPa $\sqrt{m}$/s)	Pulse [μs]	Fracture
P1	18.09	88	5.90	2.10×10^5	70	M
P2	18.25	88	4.25	1.52×10^5	70	M
P3	18.43	84	4.59	1.91×10^5	70	M
P4	18.17	static	2.27	1.00×10^{-2}	none	M
P5	18.24	static	2.18	9.20×10^{-3}	none	M
P6	20.20	88	4.66	1.66×10^5	70	H
P7	18.18	105	2.32	7.73×10^4	70	M
P8	18.05	123	2.17	4.52×10^4	70	M
P9	18.20	79	6.15	1.58×10^5	70	H
P10	18.00	117	5.29	1.12×10^5	350	H
P11	16.40	105	3.14	9.00×10^4	350	M
P12	16.20	104–96	2.55–1.56	8.20×10^4	350	M–M
P13	16.30	124–120	3.62–3.74	7.07×10^4	30	M–M
P14	16.50	108	3.79	1.15×10^5	350	M
P15	16.30	122	3.09	5.94×10^4	30	M
P16	16.03	140–120	5.44–5.87	8.07×10^4	350	H–H
P17	16.23	126–96	13.5--8.64	2.17×10^5	350	H–M

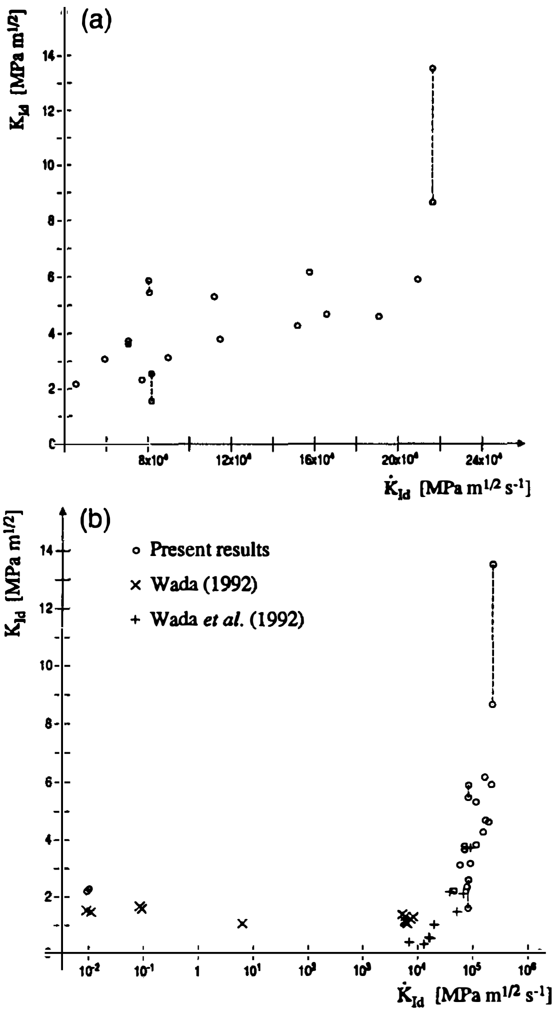

Fig. 4. (a) Dynamic fracture toughness of PMMA as a function of the stress intensity rate (dashed lines connect readings from the fracture gage on each side of the specimen). (b) Present results together with previously reported results.

in the vicinity of the notch-tip, following the terminology of Ravi-Chandar and Knauss (1984). We have divided this aspect into 'mirror/mist' and 'hackle' class, respectively, since the visual distinction between 'mirror' and 'mist' was somewhat tricky in our specimens. However, the point here is whether or not some 'hackles' can be observed in the vicinity of the crack-tip on an otherwise smooth fracture surface. This very simple classification shows a trend for 'hackles' to appear when the dynamic fracture toughness is of the order of 5 MPa $\sqrt{m}$. Such a smooth hierarchic transition of 'mirror to mist to hackles' for increasing stress intensities was reported by Ravi-Chandar and Knauss (1984). Among the four specimens tested with a double fracture gage system, two exhibit some dispersion in the measured toughness (P12 and P17) and two yield very close values (P13 and P16). Of these specimens, P17 exhibits a marked patch of 'hackles' on half the specimen thickness corresponding to the higher fracture toughness.

4.2.2. Microscopic

The fracture surfaces of several specimens were examined using light and scanning electron microscopy. Two distinct zones were examined, namely the initiation (close to the notch-tip) and propagation zone (about 10 mm farther), as shown in Figs. 5 and 6.

For the initiation zone, the statically (SL) and the dynamically loaded (DL) specimens exhibit the commonly observed feature of conical markings (C). However, for the DL specimen an additional zone of rough features (R), several hundred microns wide, can be observed as inserted between the notch-tip and the zone of conical markings. This rough area is typical of dynamic loading and is not observed in statically loaded specimens.

Further along the crack path, in the propagation zone, the fracture surface looks featureless at low (optical) magnifications. When examined at higher magnifications, the fracture surfaces of SL and DL specimens do not differ markedly even at high magnifications as shown in Fig. 7. It thus seems that the propagation zone does not contain in itself enough information to allow easy discrimination between statically and dynamically loaded specimens.

5. Discussion

The framework of the path independent H-integral and the CCS has been applied to the investigation of dynamic crack initiation in commercial PMMA specimens. This concept is relatively easy to use and can thus be applied to 'large-scale' testing of a given

(a)

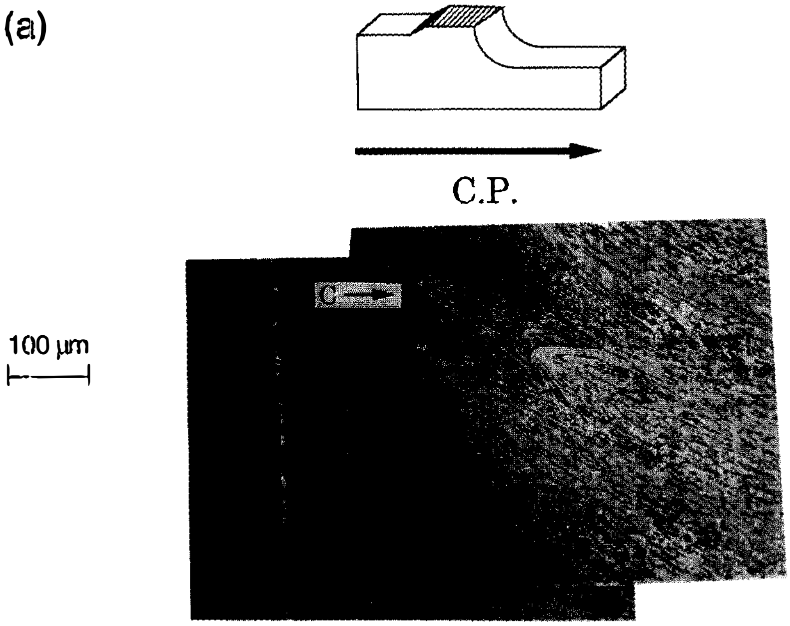

P5: KIc = 2.18 MPa√m

STATIC

(b)

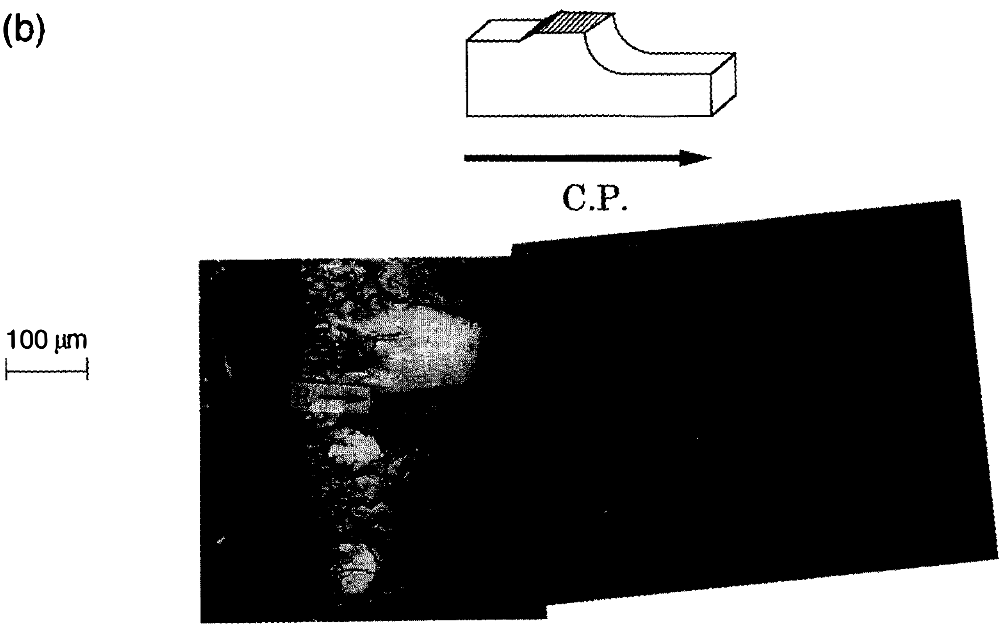

P14: KId = 3.79 MPa√m

$\dot{K}$Id = 1.15x10^5 MPa√m/s

DYNAMIC

Fig. 5. (a) Optical fractograph of a statically loaded specimen. Note the conical markings (C) in the vicinity of the notch front. (b) Optical fractograph of a dynamically loaded specimen. Note the presence of a rough zone (R) between the notch front and the conical markings.

Table 3
Dynamic fracture toughness $K_{\mathrm{Id}}^{\mathrm{c}}$ and average initial crack velocity $\bar{v}$

Specimen	$K_{\mathrm{Id}}^{\mathrm{c}}$ (MPa $\sqrt{\mathrm{m}}$)	$\bar{v}$ (m/s)
P8	2.17	150.2
P6	4.66	235.5
P9	6.15	306.2

material. This is an advantage in comparison with other methods may require more sophisticated equipment and processing of the results.

A total of 17 specimens have been tested: 2 were quasi-statically loaded until the crack propagated and the other 15 were stress wave loaded at various stress intensity rates. It must be noted that for PMMA, the fracture propagation stage is inherently unstable (at least in the range of loading rates investigated) so that the main difference between the two groups lies in the initiation phase of the crack.

The experimental results show that fracture is due to purely transient effects in the sense that the specimen fractures shortly after the stress wave has loaded the crack, at a stage where the forces on both sides of the CCS are completely different.

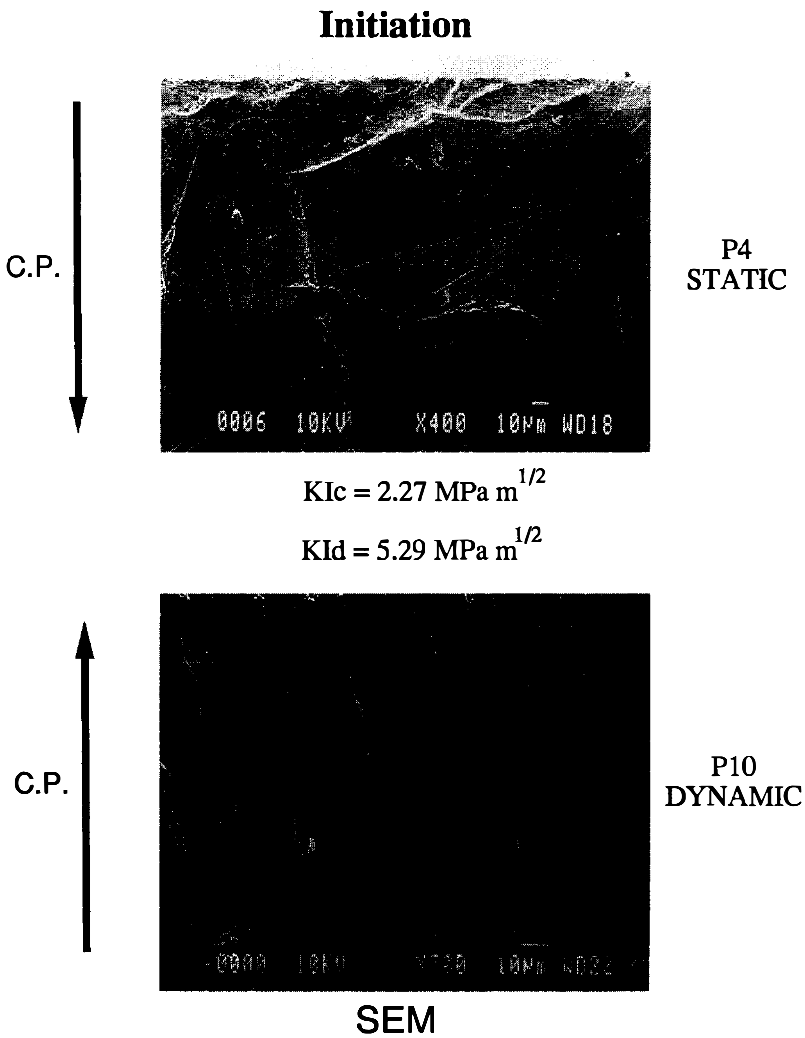

Fig. 6. Scanning electron fractographs taken in the vicinity of the notch front of a statically and a dynamically loaded specimen. Note the marked roughness characteristic of dynamic loading.

All specimens but one (P17) fractured in what appears to be mode I as evidenced from the straight crack path right at initiation. Therefore, in these experiments, the minor mode II component does not seem to affect the initiation process. The mode I fracture toughness (the mode I SIF at fracture) is observed to increase markedly with the stress intensity rate of roughly 2 MPa $\sqrt{m}$ at quasi-static loading rates to more than 5 MPa $\sqrt{m}$ at stress intensity rates of up to 10^5 MPa $\sqrt{m}$/s.

These values and their trend correspond to the results reported by other researchers who used a different framework consisting of one point bend experiments and hybrid experimental/numerical calculations. Therefore the present framework provides results which are consistent with previously reported results. However, our experimental setup allowed for higher stress intensity rates thereby providing additional points.

The dependence of K_{Id}^c on $\dot{K}_{Id}$ is not uncommon

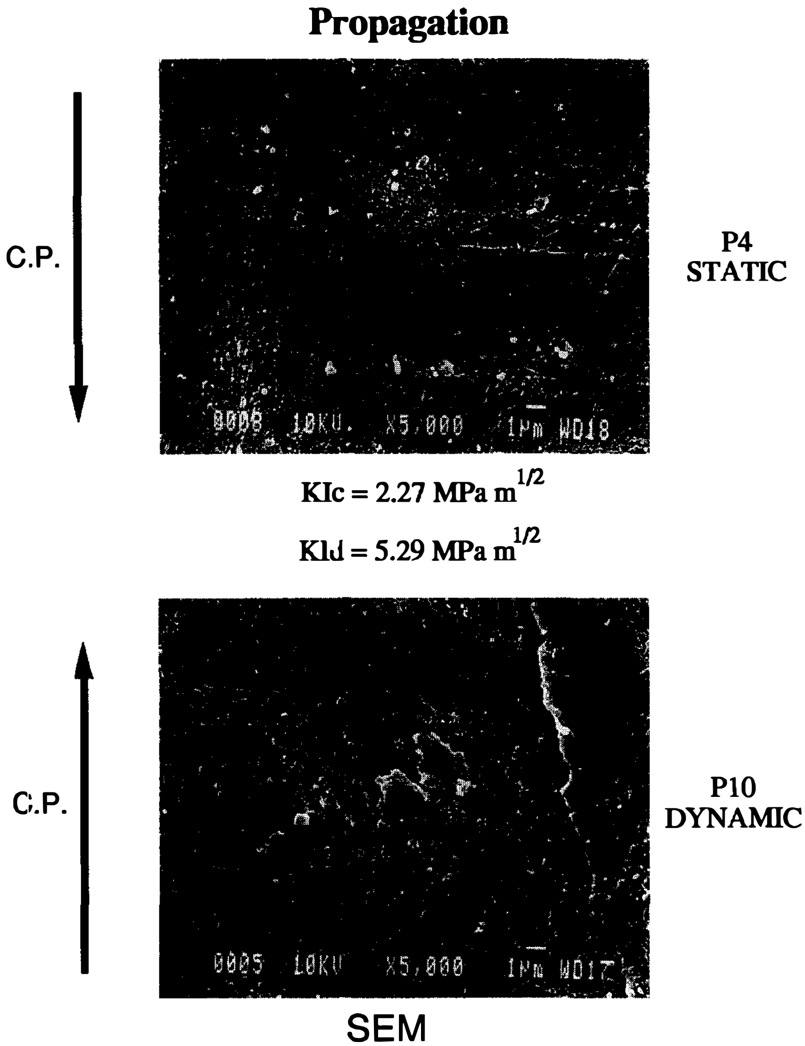

Fig. 7. Scanning electron fractographs taken about 10 mm away from the notch front of a statically and a dynamically loaded specimen. Note the lack of distinctive features on each fractograph.

for polymers (see Ravi-Chandar and Knauss, 1984) as well as for metals (see, e.g. Couque et al., 1994; Klepaczko, 1990). Whereas the mechanisms underlying this observed dependence are not clear (Aoki, 1988), two important factors have been proposed. The first relates to the postulated 'incubation time' required for the crack to initiate under transient loading (Shockey et al., 1983). The second suggests the operation of different fracture micromechanisms under static and dynamic loading (Ravi-Chandar and Knauss, 1984).

Fractographic examination in the propagation zone showed relatively similar features for statically and dynamically loaded specimens. As previously mentioned the fracture process is inherently unstable, i.e. once the crack initiated it will not arrest. Consequently, one should not expect to observe a marked difference between the two specimens at this stage of the crack propagation.

By contrast, the fractographic observations show that stress wave loading is characterized by a zone of marked roughness which is also visible at low magnifications. It appears that this zone is the most noticeable fractographic difference between dynamically and statically loaded specimens. To account for this distinct crack initiation phenomenon, it can be proposed that such zone results from the simultaneous nucleation of several microcracks along the notch front. The stress intensity factor is a macroscopic parameter which does not account, in our approach, for local phenomena of this kind. Therefore the stress intensity factor will continuously increase during the finite time required for these microcracks to coalesce and form a single crack front. Such mechanism seems consistent with both the concept of 'incubation time' and the reported observations of increasing surface roughness with the increasing stress intensity factor by Ravi-Chandar and Knauss, 1984.

Furthermore, it should be emphasized that this initial surface roughness is not observed exclusively in PMMA. In a series of experiments to be reported in a future paper, the very same features were observed to characterize dynamic crack initiation in glass. It thus appears that the nature of dynamic crack initiation mechanism(s) need further experimental characterization.

Finally, one specimen failed by kinked crack initiation. This specimen was loaded at the highest stress intensity rate in this series of experiments. The appearance of a kinked crack suggests that the minor mode II component played a role in this specific experiment causing mixed mode initiation. This aspect of dynamic crack initiation will be addressed in a future paper dedicated to this subject.

6. Conclusions

The dynamic fracture toughness of PMMA has been measured using CCS specimens and the H-integral concept. A relatively large sample size could be tested thanks to the simple experimental procedure adopted. Mode I and mode II contributions have been identified and mode I has been determined to be the major crack opening mode. This study shows that the fracture toughness of PMMA increases markedly with stress intensity rates in excess of 5.0×10^4 MPa $\sqrt{\text{m}}$/s. This observation is consistent with previous results obtained using a different approach and it extends the range of available experimental data.

The variations of the dynamic fracture toughness correlate qualitatively with the visual aspect of the fracture surfaces. A characteristic rough zone is observed on the fracture surface in the vicinity of the notch front of dynamically loaded specimens. Consequently, it is suggested that dynamic crack initiation in PMMA occurs by the possible nucleation of several microcracks along the notch front. In such case a finite time is required for their coalescence during which the stress intensity factor(s) may increase markedly.

References

Aoki, S. (1988), On the mechanics of dynamic fracture, *JSME Int. J., Ser. I* 31(3), 487–499.

ASTM (1993), Standard test method for plane-strain fracture toughness of metallic materials, *Annual book of ASTM standards*, Vol. 03.01, ASTM, Philadelphia, PA.

Bui, H.D. and H. Maigre (1988), Facteur d'intensité des contraintes tiré des grandeurs mécaniques globales, *C.R. Acad. Sc. Paris*, 306 II, 1213–1216.

Bui, H.D., H. Maigre and D. Rittel (1992), A new approach to the experimental determination of the dynamic stress intensity factor, *Int. J. Solids Struct.* 29(23), 2881–2895.

Couque, H., C.P. Leung and S.J. Hudak, Jr. (1994), Effect of planar size and dynamic loading rate on initiation and propagation toughness of a moderate-toughness steel, *Eng. Fract. Mech.*, 47(2), 249–267.

Follansbee, P.S. (1985), The Hopkinson bar, *ASM Metals Handbook*, Vol. 9, 9th Ed., Metals Park, OH.

Gary, G. and J.R. Klepaczko (1988), DAVID: Logiciel de dépouillement de l'essai de compression par barres de Hopkinson, Ecole Polytechnique, Université de Metz.

Giovanola, J.H. (1986), Investigation and application of the one-point-bend test, *ASTM STP 905*, Philadelphia, PA.

Kalthoff, J.F. (1990), Experimental fracture dynamics, in: ed. J.R. Klepaczko, *Crack Dynamics in Metallic Materials*, Springer-Verlag, Wien, pp. 69–253.

Kalthoff, J.F. and R. Podleschny (1992), On the nonsymmetry of the loading condition in Izod-type impact test configurations, in: ed. I. Maekawa, *Proc. of the Int. Symp. on Impact Eng.*, Sendai, pp. 605–610.

Klepaczko, J.R. (1990), Dynamic crack initiation, some experimental methods and modelling, in: ed. J.R. Klepaczko, *Crack Dynamics in Metallic Materials*, Springer-Verlag, Wien, pp. 254–453.

Kobayashi, A.S. (1987), *Handbook on Experimental Mechanics*, Prentice-Hall, Englewood Cliffs, NJ.

Maigre, H. and D. Rittel (1993), Mixed-mode quantification for dynamic fracture initiation: application to the compact compression specimen., *Int. J. Solids Structures*, 30(23), 3233–3244.

Ravi-Chandar, K. and W.G. Knauss (1984), An experimental investigation into dynamic fracture: II. Microstructural aspects, *Int. J. Fract.*, 25, 65–80.

Rittel, D. and H. Maigre (1993), A new approach to dynamic fracture toughness testing, in: ed. A. Shukla, *Novel Experimental Techniques in Fracture Mechanics*, ASME-AMD Vol. 176, New York, NY, pp. 173–185.

Maigre, H. and D. Rittel (1995), Dynamic fracture detection using the force-displacement reciprocity: application to the compact compression specimen, *Int. J. Fract.*, 73, 67–79.

Rittel, D., H. Maigre, and H.D. Bui (1992), A new method for dynamic fracture toughness testing, *Scripta Metall. Mater.*, 26, 1593–1598.

Shockey, D.A., J.F. Kalthoff and D.C., Erlich (1983), Evaluation of dynamic crack instability criteria, *Int. J. Fract.*, 22, 217–229.

Wada, H. (1992), Determination of dynamic fracture toughness for PMMA, *Eng. Fract. Mech.*, 41(6), 821–831.

Wada, H., C.A. Calder, T.C. Kennedy and M. Seika (1992), Measurement of impact fracture toughness with single point bending using air gun, in: ed. I. Maekawa, *Proc. of the Int. Symp. on Impact Eng.*, Sendai, pp. 569–574.

Zhao, H. (1992), Analyse de l'essai aux barres de Hopkinson: Application à la mesure du comportement dynamique des matériaux, *Doctoral thesis*, ENPC Paris.